Synthesis and Characterization of ABC Triblock Copolymers with Two Different Crystalline End Blocks: Influence of Confinement on Crystallization Behavior and Morphology

Holger Schmalz,[†] Armin Knoll,[‡] Alejandro J. Müller,[§] and Volker Abetz*,[†]

Makromolekulare Chemie II, Universität Bayreuth, 95440 Bayreuth, Germany; Physikalische Chemie II, Universität Bayreuth, 95440 Bayreuth, Germany; and Grupo de Polímeros USB, Departamento de Ciencia de los Materiales, Universidad Simón Bolívar, Caracas 1080-A, Venezuela

Received June 24, 2002; Revised Manuscript Received September 28, 2002

ABSTRACT: The preparation of polyethylene-*block*-poly(ethylene-*alt*-propylene)-*block*-poly(ethylene oxide) (PE-*b*-PEP-*b*-PEO) triblock copolymers by homogeneous catalytic hydrogenation of the precursor poly(1,4-butadiene)-*block*-poly(1,4-isoprene)-*block*-poly(ethylene oxide) (PB-*b*-PI-*b*-PEO) triblock copolymers, which were synthesized by sequential anionic polymerization, is described. Thermal analysis using differential scanning calorimetry (DSC) reveals differences in the crystallization behavior of the PEO and PE blocks arising from different morphological confinements active during crystallization. If the PEO block is confined into isolated spherical or cylindrical microdomains, crystallization can only be induced by high supercoolings resulting from the vast number of microdomains (spheres or cylinders) compared to the number of available heterogeneities. In contrast, crystallization of PE proceeds via heterogeneous nucleation regardless of the composition, which can be attributed to the miscibility of PEP and PE segments in the melt. Transmission electron microscopy (TEM) and scanning force microscopy (SFM) have been used to investigate the influence of different confinements, active in PE-*b*-PEP-*b*-PEO triblock copolymers, on the formed morphology. In addition, temperature-dependent imaging by hot-stage SFM measurements following the melting of PEO blocks and annealing of PE crystallites within a PE-*b*-PEP-*b*-PEO triblock copolymer will be presented.

Introduction

Crystallization within block copolymer microdomains is an issue which has attracted increasing interest in recent years mainly focusing on diblock copolymers. The structure development in semicrystalline block copolymers, especially those having microphase-separated melts, is enriched by the presence of two competing self-organizing mechanisms: microphase separation and crystallization. Depending on the segregation strength in the melt, either crystallization can be confined into lamellar, cylindrical, or spherical microdomains for strongly segregated systems, or crystallization can determine structure formation for weakly segregated or homogeneous systems. Three competing physical events determine the final microphase and crystalline morphology in amorphous−semicrystalline block copolymers: the microphase separation in the melt (order−disorder transition temperature T_{ODT}), the crystallization temperature (T_c) of the crystallizable block, and the vitrification (glass transition temperature T_g) of the amorphous block. In general, three different situations can be observed.[1] In diblock copolymers exhibiting a homogeneous melt ($T_{ODT} < T_c > T_g$), microphase separation is driven by crystallization. This results in a lamellar morphology where crystalline lamellae are sandwiched by the amorphous block layers regardless of the composition, as was shown for example for polyethylene-*block*-poly(ethylene-*alt*-propylene) (PE-*b*-PEP)[2] diblock copolymers. In weakly segregated systems ($T_{ODT} > T_c > T_g$, soft confinement) crystallization often occurs with little morphological constraint enabling a "breakout" from the ordered melt structure. As a consequence, crystallization overwrites any preexisting melt structure, and the resulting morphology is a lamellar structure.[1,3] However, confinement of crystallization within spherical or cylindrical microdomains is possible in strongly segregated systems and/or for highly entangled amorphous blocks (high molecular weight).[1,4−6] A strictly confined crystallization within microdomains is observed for strongly segregated diblock copolymers with a glassy amorphous block ($T_{ODT} > T_g > T_c$, hard confinement). The initially formed melt structure is preserved upon crystallization which was observed for instance in polystyrene (PS) and poly(ethylene oxide) (PEO) containing block copolymers[4,7,8] as well as polyethylene-*block*-poly(vinylcylcohexane) (PE-*b*-PVCH)[9] diblock copolymers.

Crystallization within block copolymer microdomains is affected not only by the strength of confinement but also by the structure of the microdomain, i.e., continuous (gyroid, lamellae) or dispersed (cylinders, spheres), and even the size of the microdomain. Chen et al.[10] observed for PB-*b*-PEO/PB blends with varying amount of polybutadiene (PB) homopolymer a decrease in T_c(PEO) with decreasing PEO content (domain size). Whereas in the blend with a lamellar structure T_c(PEO) = 30 °C, a large supercooling was necessary to induce PEO crystallization within PEO cylinders ($T_c = -25$ °C) or spheres ($T_c = -35$ °C). Similar results were obtained for other block copolymers, exhibiting confined crystallization within isolated spherical or cylindrical microdomains.[4,7,11] Confined crystallization within microdomains is often connected with a substantial decrease in crystallinity compared to the corresponding ho-

* Author to whom correspondence should be addressed.
[†] Makromolekulare Chemie II, Universität Bayreuth.
[‡] Physikalische Chemie II, Universität Bayreuth.
[§] Universidad Simón Bolívar.

10.1021/ma020983f CCC: $22.00
Published on Web 11/23/2002

mopolymers due to spatial restrictions and nucleation problems.[6−8,11−13] In contrast, for PE containing block copolymers the degree of crystallinity is independent of the type of microdomain and comparable with PE homopolymer, which might be attributed to the usually very thin PE crystals ($d \approx 5$ nm).[14,15] Crystallization can even be suppressed if the crystallizable block is confined into spheres or cylinders.[12,13]

The crystallization in polymers usually occurs by heterogeneous nucleation, homogeneous nucleation, or self-nucleation. In semicrystalline homopolymers crystallization in the bulk usually occurs on heterogeneous nuclei (catalyst debris, impurities, and other types of heterogeneities of unknown nature). In block copolymers the type of nucleation strongly depends on the type of microstructure. Crystallization in large or continuous domains is mostly induced by heterogeneous nucleation, because the probability that a heterogeneity is located within the crystallizable domain is large. However, crystallization in small isolated microdomains (spheres, cylinders) either proceeds in a fractionated manner, i.e., several crystallization exotherms are observed in DSC, or can only be induced by homogeneous nucleation.[4,7,10,11,13] Microdomains that contain the heterogeneities usually active at low supercoolings in the bulk polymer will crystallize at identical temperatures compared to the case of the bulk polymer. If less efficient heterogeneities are present in some microdomains, a larger supercooling is necessary to induce crystallization. Those microdomains that do not contain any heterogeneity will only be able to nucleate homogeneously (if the interphase does not affect the nucleation process). Especially in block copolymers, where the crystallizable block is confined into small isolated microdomains (spheres, cylinders), the number density of isolated microdomains is significantly higher than the number of available heterogeneities, thus favoring homogeneous nucleation.[4]

Besides the vast number of publications on amorphous ABC triblock copolymers, there have been comparatively fewer publications on ABC triblock copolymers with crystallizable blocks. Among them are reports on polystyrene-*block*-polybutadiene-*block*-poly(ϵ-caprolactone) (PS-*b*-PB-*b*-PCL) and their hydrogenated analogues (PS-*b*-PE-*b*-PCL) in which a complex interplay between microphase separation and crystallizability has been found.[4,16−18] Among others, there have been also investigations on polystyrene-*block*-polyisoprene-*block*-poly(ethylene oxide) (PS-*b*-PI-*b*-PEO)[19] and linear[7] as well as star-shaped[20] PS-*b*-PEO-*b*-PCL triblock copolymers.

In this contribution we will describe the synthesis of novel crystallizable ABC triblock copolymers comprising two different semicrystalline end blocks, polyethylene and poly(ethylene oxide), and a rubbery amorphous middle block poly(ethylene-*alt*-propylene) (PE-*b*-PEP-*b*-PEO). The synthesis includes anionic polymerization of the precursor poly(1,4-butadiene)-*block*-poly(1,4-isoprene)-*block*-poly(ethylene oxide) (PB-*b*-PI-*b*-PEO) triblock copolymers followed by homogeneous catalytic hydrogenation to yield the corresponding PE-*b*-PEP-*b*-PEO triblock copolymers. The influence of different types of confinements on the crystallization of PE and PEO will be examined using differential scanning calorimetry (DSC). Morphological investigations will be presented including wide-angle X-ray diffraction (WAXD), transmission electron microscopy (TEM), and scanning force microscopy (SFM). In addition, melting of the PEO block and annealing of PE crystallites within a PE-*b*-PEP-*b*-PEO triblock copolymer upon heating will be investigated at different temperatures applying hot-stage SFM measurements.

Experimental Section

Synthesis. Solvents and monomers for anionic polymerization were purified according to common procedures described elsewhere.[21,22] The synthesis of poly(1,4-butadiene)-*block*-poly(1,4-isoprene)-*block*-poly(ethylene oxide) (PB-*b*-PI-*b*-PEO) triblock copolymers was accomplished by sequential anionic polymerization of butadiene, isoprene, and ethylene oxide in benzene at 60 °C for butadiene and isoprene and 40 °C for ethylene oxide using *sec*-BuLi as initiator. Polymerization of ethylene oxide in the presence of a lithium counterion was realized by using the recently established strong phosphazene base *t*-BuP_4 (Fluka, 1 M in hexane, Li^+:*t*-BuP_4 = 1:1).[23−28] The reaction was completed after 3 days and terminated with a mixture of methanol/acetic acid (1/5: v/v) followed by precipitation in methanol. In our notation ($A_xB_yC_z^m$), the subscript numbers denote the mass fraction in percent and the superscript gives the number-averaged molecular weight M_n in kg/mol of the block copolymer.

Hydrogenation. The PE-*b*-PEP-*b*-PEO triblock copolymers were synthesized by hydrogenation of the corresponding precursor PB-*b*-PI-*b*-PEO triblock copolymers. Homogeneous catalytic hydrogenation was carried out in degassed toluene (1.5−2 wt % solution of the triblock copolymer) at 100 °C and 90 bar H_2 pressure for 3−4 days using the Wilkinson catalyst $(Ph_3P)_3Rh(I)Cl$ (Aldrich, 1 mol % with respect to the number of double bonds). Under the used conditions the PB block gets completely hydrogenated, and the PI block shows an almost complete saturation with ca. 1% residual double bonds as revealed by ^1H NMR. Purification was accomplished by precipitation into cold acetone followed by further purification in order to remove residual Wilkinson catalyst by refluxing a toluene solution with a small amount of concentrated hydrochloric acid, again followed by precipitation into cold acetone. Further purification was necessary due to the strong tendency of PEO to bind residual Wilkinson catalyst. Alternatively, several triblock copolymers were hydrogenated using diimide, generated in-situ by the thermolysis of *p*-toluenesulfonyl hydrazide (TSH, Fluka).[29] The triblock copolymers were purified by filtration over basic aluminum oxide in order to remove residual *p*-toluenesulfonic acid (thermolysis product of *p*-toluenesulfonyl hydrazide) followed by precipitation into cold acetone. This method resulted in a complete hydrogenation of the PB block, whereas the PI block exhibits a degree of hydrogenation of ca. 70%.

Size Exclusion Chromatography (SEC). SEC experiments were performed on a Waters instrument calibrated with narrowly distributed polystyrene standards at 30 °C.[22] Molecular weights of the PB precursors were calculated from the apparent values obtained by SEC using given K and α values for PS and PB resulting in the equation $M_n(PB) = 0.696 \cdot M_n(PS)^{0.985}$ (Mark−Houwink−Sakurada relation).[30]

Differential Scanning Calorimetry (DSC). For thermal analysis a Perkin-Elmer DSC 7 with a CCA 7 liquid nitrogen cooling device was used. For all measurements a two-point calibration with decane and indium was applied. All experiments were performed at a scanning rate of 10 °C/min. The displayed heating traces correspond to the second heating run in order to exclude effects resulting from any previous thermal history of the samples. Because of the vicinity of the melting endotherms of PEO and PE (problems involved in the baseline definition for the PE endotherm), the degree of crystallinity for the PE blocks was extracted from the heat of crystallization. The degree of crystallinity for the PEO blocks was determined from the heat of fusion.

Wide-Angle X-ray Diffraction (WAXD). WAXD investigations of $E_{19}EP_{40}EO_{41}^{138}$ were performed on a Bruker-AXS D8 Advance diffractometer equipped with a scintillation counter and a Goebel mirror using Cu Kα radiation at room

Scheme 1. Synthesis of Poly(1,4-butadiene)-*block*-poly(1,4-isoprene)-*block*-poly(ethylene oxide) Triblock Copolymers (PB-*b*-PI-*b*-PEO) by Sequential Anionic Polymerization

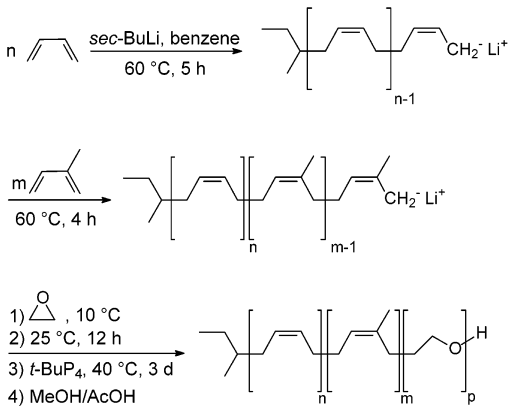

temperature. Sample preparation was accomplished by compression molding between PTFE plates at 140 °C followed by cooling to room temperature.

Transmission Electron Microscopy (TEM). The bulk morphology of PE-*b*-PEP-*b*-PEO triblock copolymers was examined by bright field TEM using a Zeiss CEM 902 electron microscope operated at 80 kV. Films (around 0.5 mm thick) were prepared by casting from a 3 wt % solution of the triblock copolymer in toluene at 70 °C in order to avoid gelation upon solvent evaporation. After complete evaporation of the solvent (ca. 1 week), the films were slowly cooled to room temperature to induce crystallization of the PE and PEO blocks followed by further drying under vacuum at 40 °C for 2 days. Thin sections were cut at − 130 °C using a Reichert-Jung Ultracut E microtome equipped with a diamond knife. Staining of amorphous PEO and PEP segments was accomplished by exposure of the thin sections to RuO_4 vapor for 30−40 min. Because of local conformational constraints active at microdomain interphases (reduced density), a preferential staining of the PEO/PEP microdomain interphase is observed. For the triblock copolymer $E_{19}EP_{40}EO_{41}$[138], which has been synthesized by hydrogenation of the corresponding PB-*b*-PI-*b*-PEO triblock copolymer using TSH, OsO_4 vapor was used as staining agent (exposure for 1 min). Here, the PEP block contains ca. 30% residual double bonds (see Hydrogenation section), which can be selectively stained using OsO_4.

Scanning Force Microscopy (SFM). Scanning force microscopy images were taken on a Digital Instruments Dimension 3100 microscope operated in TappingMode (free amplitude of the cantilever ≈20 nm; set point ratio ≈0.95). Measurements were performed on thin films prepared on polished silicon wafers by dip- or spin-coating from a 2 wt % solution of the triblock copolymer in toluene. For temperature-dependent measurements a D3/D5 SPC01 hot stage from Digital Instruments was used.

Results and Discussion

Synthesis. The PE-*b*-PEP-*b*-PEO triblock copolymers were prepared by homogeneous catalytic hydrogenation of the corresponding PB-*b*-PI-*b*-PEO triblock copolymers.

The synthesis of PB-*b*-PI-*b*-PEO triblock copolymers was accomplished by sequential anionic polymerization of butadiene, isoprene, and ethylene oxide in benzene as depicted in Scheme 1. The polymerization of butadiene and isoprene in benzene at 60 °C leads to a preferential 1,4-addition (Table 1), which especially for butadiene is indispensable to get the corresponding "pseudo polyethylene" structure after hydrogenation. Polymerization in a one-step procedure was realized using the recently established strong phosphazene base

Table 1. Molecular Weight Characterization and Microstructure of PB-*b*-PI-*b*-PEO Triblock Copolymers

			PB-block[c]		PI-block[c]		
triblock copolymer	M_n[a] [kg/mol]	M_w/M_n[b]	% 1,4	% 1,2	% 1,4	% 1,2	% 3,4
$B_{24}I_{56}EO_{20}$[67]	67.3	1.01	89	11	88	6	6
$B_{11}I_{70}EO_{19}$[120]	120	1.01	88	12	92	4	4
$B_{17}I_{57}EO_{26}$[130]	130	1.01	89	11	92	4	4
$B_{19}I_{39}EO_{42}$[135]	135	1.02	89	11	92	4	4

[a] Determined by ^{1}H NMR spectroscopy using the molecular weight of the PB precursor obtained by SEC in THF calibrated against PS standards; for PB the molecular weight was calculated from the apparent value obtained by SEC using the equation $M_n(PB) = 0.696\ M_n(PS)^{0.985}$. [b] Determined by SEC in THF calibrated against PS standards. [c] Determined by ^{1}H NMR spectroscopy in $CDCl_3$.

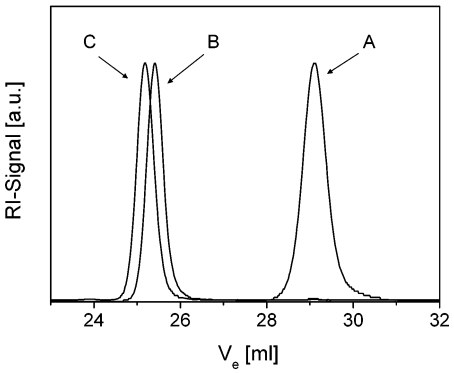

Figure 1. SEC traces of a synthesized PB-*b*-PI-*b*-PEO (C) triblock copolymer including the PB (A) and PB-*b*-PI (B) precursors using THF as eluent and toluene as internal standard.

t-BuP_4,[23−28] enabling polymerization of ethylene oxide in the presence of a Li^+ counterion. SEC investigations (Figure 1) show that the reaction proceeds without any termination, resulting in narrowly distributed PB-*b*-PI-*b*-PEO triblock copolymers (Table 1). Kinetic investigations on the ethylene oxide polymerization with organolithium initiators in the presence of the phosphazene base *t*-BuP_4 revealed the existence of an induction period.[31,32] As a result, reaction times of 2−3 days are necessary to get 100% conversion.

Homogeneous catalytic hydrogenation was carried out in toluene using Wilkinson catalyst $(Ph_3P)_3Rh(I)Cl$ (Scheme 2). The efficiency of the hydrogenation reaction was verified by ^{1}H NMR spectroscopy showing a complete hydrogenation of the PB block and an almost complete saturation of the PI block with ≤1% residual double bonds (results not shown). For several triblock copolymers an alternative hydrogenation method was applied using *p*-toluenesulfonyl hydrazide (TSH). Using this method, a complete saturation of the PB block can be achieved, whereas the PI block exhibits a degree of hydrogenation of only ca. 70% due to sterical hindrance involved in the hydrogenation reaction.

Differential Scanning Calorimetry: PB-*b*-PI-*b*-PEO. Table 2 summarizes the thermal properties of the PB-*b*-PI-*b*-PEO and the corresponding hydrogenated PE-*b*-PEP-*b*-PEO triblock copolymers. The PB-*b*-PI-*b*-PEO triblock copolymers exhibit a glass transition temperature at ≈−70 °C corresponding to a mixed phase of PB and PI. Consequently, the PB-*b*-PI-*b*-PEO triblock copolymers might be considered as diblock copolymers consisting of a PEO phase and a mixed PB/PI phase. The PEO blocks display a melting endotherm

Scheme 2. Synthesis of PE-*b*-PEP-*b*-PEO Triblock Copolymers via Homogeneous Catalytic Hydrogenation of the Corresponding PB-*b*-PI-*b*-PEO Triblock Copolymers Using Wilkinson Catalyst

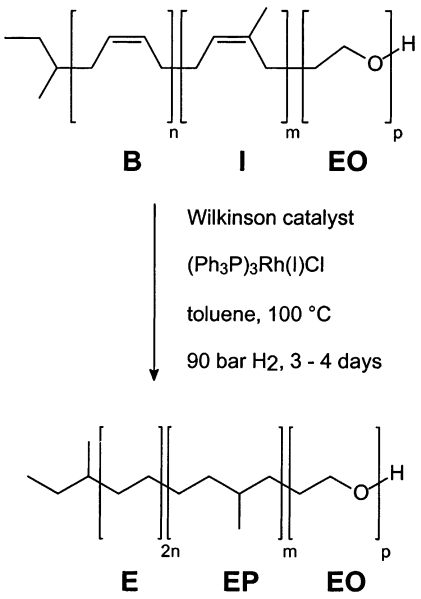

at approximately 60−66 °C and a degree of crystallinity of $\alpha \approx 70-85\%$, whereby the melting temperature increases with increasing PEO content (Figure 2A, Table 2). The degree of crystallinity was calculated assuming a heat of fusion for PEO of $\Delta H_m^0 = 196.6$ J/g.[33] The crystallization of PEO occurs in all triblock copolymers with PEO contents <30 wt % at about −20 °C. However, the triblock copolymer with 26 wt % PEO exhibits an additional small exotherm at 16 °C (Table 2, Figure 2B). From composition, a cylindrical PEO microstructure might be assumed and has been observed in the corresponding hydrogenated triblock copolymer $E_{18}EP_{57}EO_{25}^{133}$ (see discussion on $E_{18}EP_{57}EO_{25}^{133}$, Figure 4A). Thus, the high-temperature exotherm ($T_c = 16$ °C) might be attributed to heterogeneous crystallization of PEO within interconnected PEO cylinders and the low-temperature exotherm ($T_c = -21$ °C) to crystallization within isolated cylinders. In general, the crystallization exotherm exhibits a slight shift to higher temperatures with increasing PEO content and/or molecular weight of the PEO block. The observed crystallization temperatures in PB-*b*-PI-*b*-PEO triblock copolymers with PEO contents <30 wt % are significantly lower compared to the values observed in PEO homopolymer ($T_c \approx 40$ °C).[4] This is a direct result of the vast number density of PEO microdomains ($\approx 10^{16}$ spheres/cm^3 or $\approx 10^{14}$ cylinders/cm^3) for $B_{11}I_{56}EO_{19}^{120}$ assuming a spherical ($d \approx 20$ nm, see SFM section) or cylindrical microstructure (expecting an average length of 1 μm for the PEO blocks) compared to the number density of heterogeneous nuclei usually present in PEO homopolymers ($\approx 10^5$ nuclei/cm^3, for a spherulite radius of 100 μm[10]).[4] Similar results have been observed by Chen et al. for PB-*b*-PEO/PB blends.[10] The authors found that the crystallization temperature strongly depends on the volume of the dispersed PEO phase. If the PEO blocks are confined into cylinders, crystallization occurs at approximately −25 °C, and for PEO spheres the crystallization temperature shifts to even lower temperatures (≈−34 °C).

As a consequence of confinement, crystallization cannot proceed via heterogeneous nucleation, which is reflected in the observed large supercoolings necessary for crystallization in PB-*b*-PI-*b*-PEO triblock copolymers (PEO content < 30 wt %). However, the crystallization temperatures observed for homogeneous nucleation in other PEO containing block copolymers ($T_c \approx -40$ °C)[7] are significantly smaller than the observed values. Accordingly, the observed crystallization behavior cannot be attributed to a homogeneous nucleation mechanism. Self-nucleation experiments show that domain II (self-nucleation domain) is completely absent for the PEO block in PB-*b*-PI-*b*-PEO triblock copolymers (PEO content < 30 wt %).[34] Thus, nucleation induced by less efficient heterogeneities can be excluded, and the observed crystallization behavior might be attributed to a nucleating property of the microdomain interphase. A similar result was obtained in self-nucleation experiments on the hydrogenated triblock copolymer $E_{24}EP_{57}EO_{19}^{69}$.[4]

In $B_{19}I_{39}EO_{42}^{135}$ the PEO block exhibits peak crystallization temperatures at 37 and 20 °C, which are close to the values observed in PEO homopolymer (Table 2, Figure 2B). From composition a lamellar microdomain structure might be expected and has been observed by TEM investigations exhibiting crystalline PEO lamellae within a matrix of the miscible PB and PI segments (results not shown). However, a cylindrical microphase cannot completely be excluded due to uncertainties involved in the staining technique and problems involved in the preparation of thin sections (cutting artifacts) due to the very soft samples (see also discussion on the corresponding hydrogenated triblock copolymer). The observation of a double exotherm might be attributed to crystallization within interconnected (higher T_c) and isolated (lower T_c) PEO lamellae, as was also concluded from the occurrence of a double exotherm in lamellar PE-*b*-PVCH diblock copolymers.[9] In conclusion, crystallization of PEO within $B_{19}I_{39}EO_{42}^{135}$ occurs with little morphological restrictions within lamellar PEO microdomains via heterogeneous nucleation.

PE-*b*-PEP-*b*-PEO. Any effects on the crystallization behavior of the PE-*b*-PEP-*b*-PEO triblock copolymers arising from residual Wilkinson catalyst could be excluded due to the applied purification procedure. The influence of Wilkinson catalyst debris on the crystallization of PEO is discussed elsewhere.[34] The PE-*b*-PEP-*b*-PEO triblock copolymers show melting endotherms for PE and PEO indicating microphase separation even for low molecular weights, which in the case of PE is induced by crystallization (Table 2, Figure 3A). Because of the small segmental interaction parameter χ of 0.007 at 120 °C for PE and PEP,[35] crystallization of PE is expected to occur from a homogeneous mixture of PE and PEP segments.[2,36−38] In contrast, crystallization of the strongly incompatible PEO segments is confined into microphase-separated PEO domains.

The crystallization behavior of the PEO block within purified PE-*b*-PEP-*b*-PEO triblock copolymers is comparable to that discussed for the corresponding PB-*b*-PI-*b*-PEO triblock copolymers (Table 2). Crystallization of PEO in $E_{18}EP_{57}EO_{25}^{133}$ occurs nearly completely at 27 °C, whereas in the corresponding $B_{17}I_{57}EO_{26}^{130}$ triblock copolymer the major fraction of PEO crystallizes at −21 °C (Table 2, Figure 2B, 3B). Since effects from catalyst residues can be excluded, this effect might be attributed to differences in the cylindrical PEO microdomain structure, i.e., strongly interconnected PEO cylinders in $E_{18}EP_{57}EO_{25}^{133}$ favoring heterogeneous

Table 2. DSC Data for PB-*b*-PI-*b*-PEO and PE-*b*-PEP-*b*-PEO Triblock Copolymers[a]

triblock copolymer[b]	T_g [°C]	T_m(PEO) [°C]	T_{c1}(PEO)[c] [°C]	T_{c2}(PEO) [°C]	α(PEO) [%]	T_m(PE) [°C]	T_c(PE) [°C]	α(PE) [%]
$B_{24}I_{56}EO_{20}^{67}$	−69.5[d]	60.5	−23.9	–	84.5	–	–	–
$B_{11}I_{70}EO_{19}^{120}$	−65.9[d]	60.0	−22.2	–	71.4	–	–	–
$B_{17}I_{57}EO_{26}^{130}$	−67.5[d]	63.2	−21.0 (83)	16.1	70.4	–	–	–
$B_{19}I_{39}EO_{42}^{135}$	−68.7[d]	65.9	−25.0 (2)	37.5/19.8	77.8	–	–	–
$E_{24}EP_{57}EO_{19}^{69}$ (5.8)	−57.4	58.9	−26.4	–	80.2	93.4	66.5	27.4
$E_{11}EP_{71}EO_{18}^{123}$ (6.4)	−56.4	59.7	−25.4	–	65.0	89.0	50.0	38.1
$E_{11}EP_{71}EO_{18}^{123}$ [e]	−59.1	60.8	−25.3	–	70.3	89.6	53.5	37.9
$E_{18}EP_{57}EO_{25}^{133}$ (5.8)	−56.8	60.0	−21.1 (4)	26.8	56.9	92.9	64.6	21.2
$E_{19}EP_{40}EO_{41}^{138}$ (5.8)	−57.1	63.9	−24.0 (6)	37.6/23.6	72.1	94.4	69.4	20.3
$E_{19}EP_{40}EO_{41}^{138}$ [e]	−59.3	64.8	−22.6 (1)	39.0/22.6	69.9	94.0	71.4	19.8

[a] T_m = melting point of corresponding block (peak maximum), T_c = crystallization temperature of corresponding block (peak maximum), α = degree of crystallinity, and T_g = glass transition temperature. [b] Values in parentheses give the content of ethyl branches within the PE block in mol %. [c] Values in parentheses give the fraction of crystallinity (in %). [d] Glass transition temperature of the mixed PB/PI phase. [e] Triblock copolymer was hydrogenated using *p*-toluenesulfonyl hydrazide.

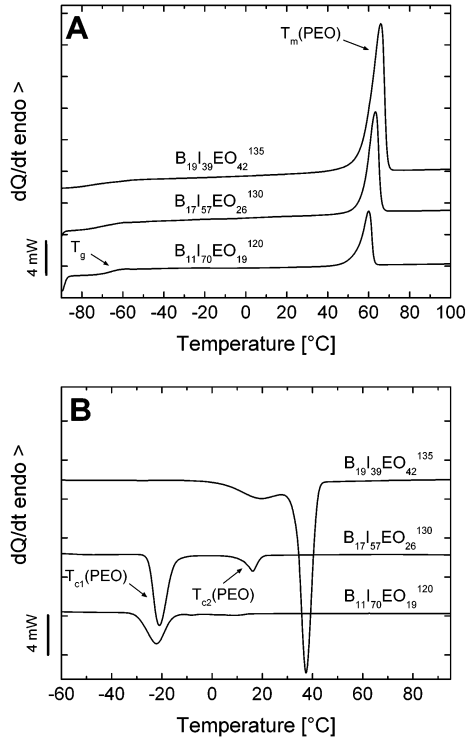

Figure 2. DSC heating (A) and cooling (B) traces for several PB-*b*-PI-*b*-PEO triblock copolymers.

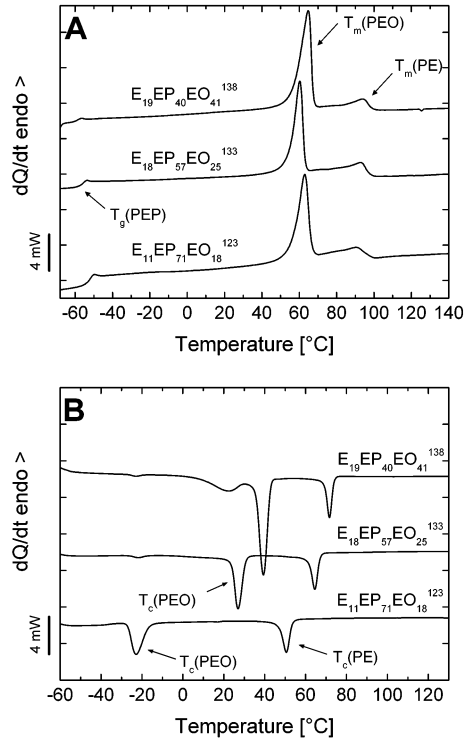

Figure 3. DSC heating (A) and cooling (B) traces for several PE-*b*-PEP-*b*-PEO triblock copolymers.

nucleation. Figure 4A shows the corresponding TEM micrograph obtained by staining a thin section of the sample with RuO_4 vapor. Thin sections were cut from a film cast from toluene solution at 70 °C, followed by slowly cooling to room temperature in order to induce crystallization of PE and PEO. The PEO blocks exhibit a distorted cylindrical structure (both top and side view of PEO cylinders visible), and interconnections between different PEO cylinders are clearly visible. Because of the used staining technique, the interphase between PEO cylinders and the PEP matrix gets preferentially stained. This results in the visible dark shadow surrounding the PEO cylinders, whereby the PEP matrix appears only slightly gray. Furthermore, the PEO cylinders are obviously subdivided into small spherical domains. These subdomains might be attributed to stacks of several PEO crystallites within the cylindrical PEO domains. One restriction of the used staining technique is the fact that the crystalline PE domains, which are expected to be located within the PEP matrix, cannot be visualized.

The triblock copolymer $E_{19}EP_{40}EO_{41}^{138}$ exhibits a double exotherm for PEO, which is in line with the observations in the corresponding $B_{19}I_{39}EO_{42}^{135}$ triblock copolymer (Table 2, Figure 2B, 3B). TEM investigations on the completely hydrogenated $E_{19}EP_{40}EO_{41}^{138}$ (hydrogenation with Wilkinson catalyst) show a cylindrical microdomain structure for the PEO blocks (Figure 4B). TEM investigations with lower magnifications show that the PEO cylinders can extend over several micrometers (results not shown). In contrast to the nonhydrogenated analogue showing a lamellar structure, the increased segregation strength in the hydrogenated triblock copolymer and the presence of a second crystalline block (PE) might be responsible for the change in the PEO microdomain structure. From the PEO cylinders, oriented perpendicular to the plane of observation, it can be deduced that the PEO cylinders exhibit a rectangular shape rather than a spherical shape, which might be attributed to the fact that the PEO cylinders are semicrystalline. However, because of the staining technique (RuO_4 vapor), the crystalline PE domains cannot be visualized, as only the interphase between

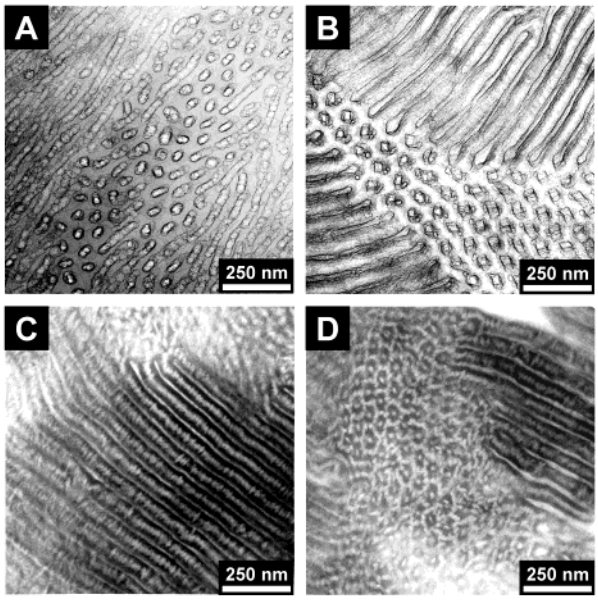

Figure 4. TEM micrographs of $E_{18}EP_{57}EO_{25}^{133}$ (A, RuO_4 staining), $E_{19}EP_{40}EO_{41}^{138}$ hydrogenated using Wilkinson catalyst (B, RuO_4 staining), and $E_{19}EP_{40}EO_{41}^{138}$ hydrogenated with TSH (C and D, OsO_4 staining).

PEO cylinders and the PEP matrix gets preferentially stained (compare with Figure 4A).

As mentioned before, hydrogenation using *p*-toluenesulfonyl hydrazide results in an incomplete hydrogenation of the PI blocks within $B_{19}I_{39}EO_{42}^{135}$. These residual double bonds can be selectively stained with OsO_4 vapor, together with amorphous PEO segments. Figure 4C,D shows TEM micrographs for $E_{19}EP_{40}EO_{41}^{138}$, prepared by hydrogenation with *p*-toluenesulfonyl hydrazide. In Figure 4C a projection along the thin white appearing PEO cylinders is shown. The fraction of PEO is apparently smaller as compared to Figure 4B. This might be attributed to the fact that only the crystalline PEO domains are visible, as the amorphous PEO segments get stained by OsO_4, too. Within the selectively stained PEP matrix (dark gray color) small white appearing domains are visible which are oriented perpendicular to the long direction of the PEO cylinders. This microphase can be attributed to PE crystallites, as crystallization of PE occurs without confinement from a homogeneous mixture of PEP and PE segments. The TEM image in Figure 4D shows a projection perpendicular to the PEO cylinder axis. From this image it can be extracted that PE crystallization is templated by the strongly segregated PEO cylinders, resulting in a hexagonally array of PE crystallites surrounding the PEO cylinders. Furthermore, the PE crystallites are apparently interconnected and form a continuous crystalline PE phase within the PEP matrix.

The PE block in PE-*b*-PEP-*b*-PEO triblock copolymers exhibits a melting temperature of approximately 90 °C and a degree of crystallinity between 20 and 38% (Table 2). The degree of crystallinity was calculated using the heat of fusion for a 100% crystalline PE of ΔH^0_m = 276.98 J/g.[30] The DSC traces in Figure 3A display a relatively broad melting endotherm for the PE block, reflecting a broad crystallite size distribution. The latter may arise from the ethyl branches within the PE block originating from the approximately 11% 1,2-units in the corresponding PB block of the non-hydrogenated triblock copolymer precursors (Table 1). PE-*b*-PEP-*b*-PEO

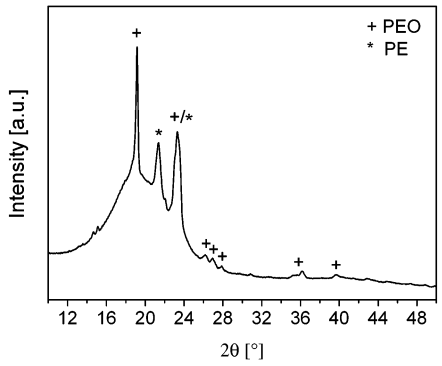

Figure 5. WAXD-pattern obtained for $E_{19}EP_{40}EO_{41}^{138}$ exhibiting reflex positions attributable to a triclinic modification of PEO and an orthorhombic modification of PE.

triblock copolymers with ca. 20 wt % PE exhibit crystallization temperatures of about 65−72 °C (Table 2, Figure 3B) reflecting a heterogeneous nucleation mechanism, since the observed values are very close to the crystallization temperature of ca. 73 °C observed in a hydrogenated polybutadiene with a similar content of ethyl branches.[4] However, the triblock copolymer $E_{11}EP_{71}EO_{18}^{123}$ exhibits a comparatively lower melting and crystallization temperature for the PE block. This might be attributed on one hand to the higher amount of ethyl branches in the PE block (Table 2), resulting in thinner crystallites (lower T_m), and on the other hand to a slightly decreased segregation strength of the PE and PEP segments arising from the lower PE content (lower T_c). Self-nucleation measurements on the PE block in PE-*b*-PEP-*b*-PEO triblock copolymers show that for all samples domain II (self-nucleation domain) is present, strongly underlining a heterogeneous nucleation mechanism.[34] In conclusion, crystallization of PE within PE-*b*-PEP-*b*-PEO triblock copolymers is induced by heterogeneous nucleation, even for very small PE contents (11−24 wt %). In contrast to the confined crystallization of PEO within isolated microdomains (for low PEO contents), crystallization of PE occurs without confinement from a homogeneous mixture of PE and PEP segments, thus enabling heterogeneous nucleation.

Wide-Angle X-ray Diffraction (WAXD). To gain more insight into the crystal structure of the crystalline PE and PEO domains, wide-angle X-ray diffraction has been used. Figure 5 shows the diffraction pattern obtained for $E_{19}EP_{40}EO_{41}^{138}$. The reflex positions at 2θ = 19°, 23°, ≈27°, 36°, and 40° reveal crystallization of PEO in its triclinic modification,[39] which has also been observed for PS-*b*-PEO and PS-*b*-PEO-*b*-PCL block copolymers.[7] PE usually shows an orthorhombic crystal structure with corresponding reflex positions at 2θ = 21° and 24°.[15,40] Comparison with Figure 5 reveals a reflex position at 2θ = 21°, corresponding to PE in its orthorhombic modification, whereas the second reflex position at 2θ = 24° is superimposed with a reflex arising from the PEO crystals. In conclusion, WAXD shows that the PE and PEO blocks within PE-*b*-PEP-*b*-PEO triblock copolymers form well-organized crystals exhibiting an orthorhombic and a triclinic crystal structure, respectively.

Scanning Force Microscopy (SFM). The influence of different confinements, being active during PE and PEO crystallization, on the formed morphology can be visualized using scanning force microscopy. The large differences in stiffness between amorphous and crystalline domains make SFM a superior tool for the inves-

tigation of semicrystalline−amorphous block copolymers, without the need of special sample preparations. Most SFM investigations have been performed on crystallizable homopolymers[41−55] or semicrystalline−amorphous diblock copolymers,[56−59] whereas only few reports concern the crystallization within semicrystalline ABC triblock copolymers.[22,60]

Parts A and B of Figure 6 show the SFM topography and phase contrast images of $E_{11}EP_{71}EO_{18}^{123}$, respectively, prepared by dip-coating from a 2 wt % solution of the triblock copolymer in toluene. Three different phases can be distinguished from the phase contrast image (Figure 6B). The bright appearing elongated domains correspond to crystalline PE lamellae viewed edge on, which are embedded in an amorphous matrix of the less bright appearing PEP blocks. (Hard materials usually induce a higher phase shift compared to soft materials.) The PE crystallites are also clearly visible in the corresponding topography image (Figure 6A). Because of the miscibility of molten PE and PEP segments, there is no confinement active during crystallization of PE. This results in the observed randomly distributed and strongly interconnected PE crystallites. Upon solvent evaporation during the dip-coating process first the PE segments start to crystallize from the homogeneous solution due to the low solubility of PE in toluene. This results in the formation of the observed continuous crystalline PE phase. This assumption is underlined by the observation that higher concentrated solutions (3−4 wt %) of the triblock copolymer form gels in toluene or *o*-xylene solutions at room temperature. As the PEO blocks are not able to crystallize at room temperature (Table 2, Figure 3B), this observation can only be explained by the formation of a continuous crystalline PE phase in the solution. Rheological investigations on a 3.6 wt % solution of $E_{11}EP_{71}EO_{18}^{123}$ in *o*-xylene reveal a gel point at ca. 49 °C upon heating attributed to the melting of interconnected PE crystallites, which in turn results in a breakup of the physical network (results not shown). In addition, a third phase can be detected in the phase contrast image (Figure 6B). The dark appearing (low phase shift) spherical domains located in between the crystalline PE lamellae, which correspond to the dark spherical domains in the topography image (Figure 6A), can be attributed to amorphous PEO domains, as the PEO blocks are not able to crystallize at room temperature (Table 2, Figure 3B).

Since the formation of a continuous crystalline PE phase is induced by the gelation of the solution upon solvent evaporation in the dip-coating process, a thin film of $E_{11}EP_{71}EO_{18}^{123}$ was prepared by dip-coating from a warm toluene solution (≈40 °C). As can be seen from the corresponding phase contrast image (Figure 6C), the crystalline PE lamellae (bright appearing domains) are more isolated and exhibit smaller lengths as compared to Figure 6B. Moreover, the morphology appears more ordered as can be seen from the homogeneously distributed spherical PEO microdomains. With respect to the composition (18 wt % PEO) PEO spheres or cylinders might be expected. The phase contrast image (Figure 6C) strongly suggests a spherical microdomain structure for the PEO block exhibiting an average diameter of 20−25 nm. However, cylindrical PEO microdomains cannot be excluded, as cylinders aligned perpendicular to the substrate surface would also result in the observation of an apparently spherical microdomain structure.

Increasing the PEO content to 41 wt % in $E_{19}EP_{40}EO_{41}^{138}$ results in a completely different morphology with respect to the PEO domains as depicted in the corresponding phase contrast image (Figure 6D). Here the PEO blocks are able to crystallize at room temperature (T_c = 38 °C, Table 2). This results in a white appearing (high phase shift) PEO phase consisting of several stacks of crystalline PEO lamellae (viewed edge on), which are located in between the less bright appearing continuous crystalline PE phase. Figure 6E,F shows the topography and phase contrast images of the same film, subjected to an annealing at 91 °C for 5 min followed by cooling at a constant rate of −5 °C/min to room temperature. At 91 °C the PEO blocks are completely molten (Table 2, Figure 3A), whereas the PE blocks show annealing as revealed by DSC measurements (results not shown).[34] Large PE crystallites grow at the expense of smaller, less stable crystallites and surrounding molten PE segments, resulting in a more uniform crystallite size distribution without destroying the continuous crystalline PE structure, as is demonstrated by the corresponding phase contrast image (Figure 6F). Upon cooling from 91 °C, the PEO blocks crystallize under the spatial confinement of the existing continuous crystalline PE phase. A comparison with the film prior to annealing (Figure 6D) reveals that the crystalline PEO domains are significantly larger, and the crystallites exhibit a higher lateral extension when the PEO blocks are allowed to crystallize from the melt.

We have followed the morphological changes upon melting of the PEO blocks and annealing of the PE crystallites in $E_{19}EP_{40}EO_{41}^{138}$ by hot-stage SFM measurements. Figure 7 shows phase contrast images of a thin film of $E_{19}EP_{40}EO_{41}^{138}$ prepared by spin-coating from a 2 wt % solution of the triblock copolymer in toluene, taken at the same spot of the film at different temperatures upon heating. At 42.7 °C, a temperature well below the melting transition of the PEO and PE blocks (Table 2, Figure 3A), the crystalline PEO and PE domains are clearly visible (Figure 7A). It should be noted that the crystalline PE domains are expected to consist of several PE crystallites with different thickness, as from DSC a broad crystallite size distribution, reflected by the broad melting transition, can be derived (Figure 3A). However, it is not possible to resolve the resulting lamellar fine structure within the PE domains at this point due to the broad crystallite size distribution. Upon heating to 60.1 °C, partial melting of the PEO block starts as can be derived from the corresponding heating trace (Figure 3A). As a consequence, the average size of crystalline PEO domains decreases, which can be deduced from the comparison of the phase contrast images taken at 42.7 and 60.1 °C (circles in Figure 7A,B). At this temperature comparatively small crystallites are already completely molten as depicted by the arrows in Figure 7A,B.

A further increase in temperature to 65.7 °C, a temperature above the observed maximum in the melting transition (T_m = 64.8 °C, Table 2), results in a complete melting of PEO crystallites, and only the crystalline PE domains (T_m = 94 °C, Table 2) remain as depicted in Figure 7C. Further heating is connected with an annealing of PE crystallites which has been derived from self-nucleation experiments (results not shown);[34] i.e., larger crystallites grow at the expense of smaller, less stable crystallites or surrounding molten PE segments. Figure 7D shows the phase contrast

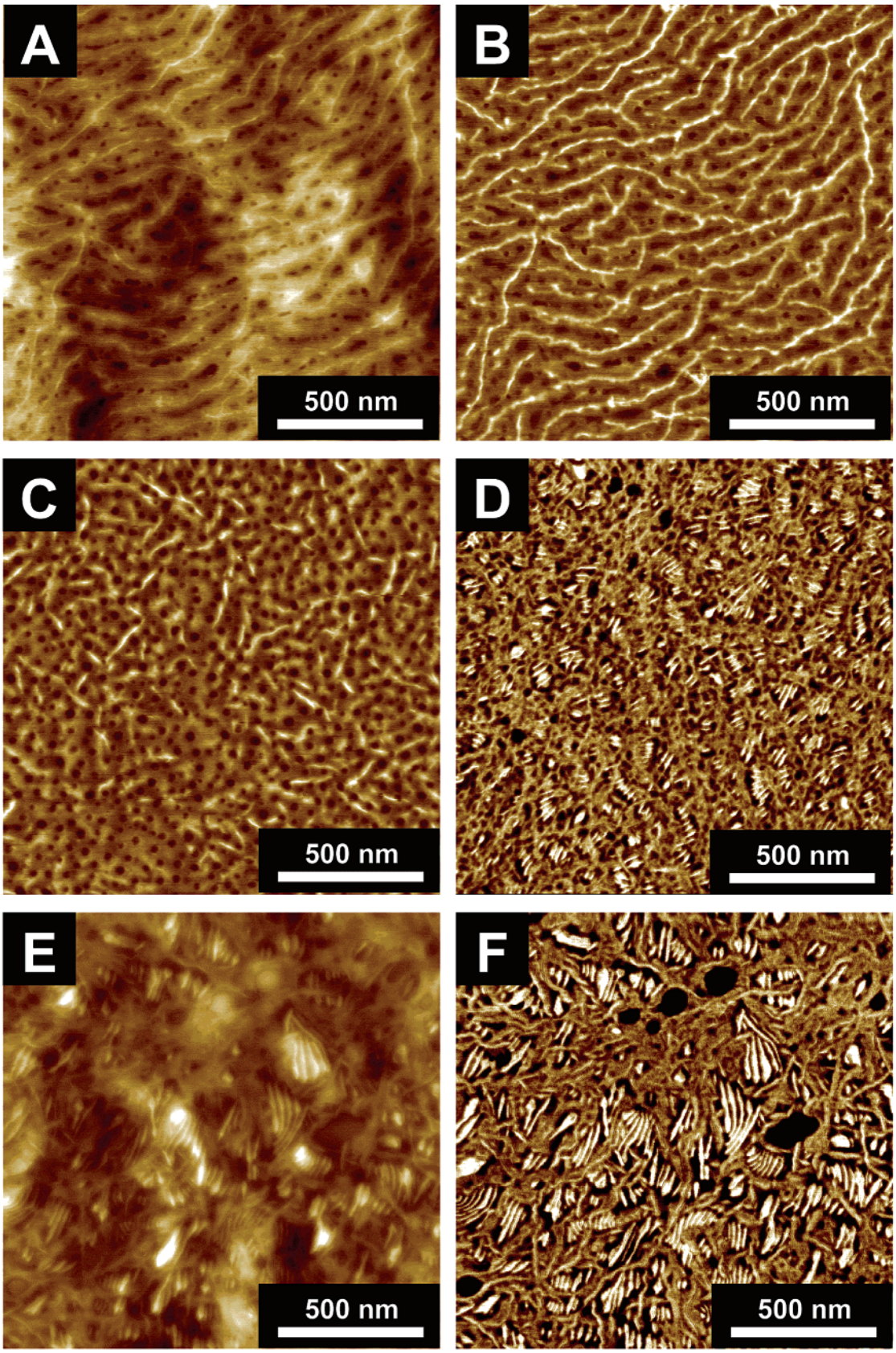

Figure 6. SFM topography and phase contrast images for $E_{11}EP_{71}EO_{18}^{123}$ (A, $z = 20$ nm; B, $z = 15°$; C, $z = 20°$: prepared from a warm toluene solution (≈40 °C)) and for $E_{19}EP_{40}EO_{41}^{138}$ before (D, $z = 20°$) and after annealing at 91 °C for 5 min (E, $z = 60$ nm; F, $z = 20°$).

image taken at 88.7 °C, a temperature revealing a large extent of annealing processes. Comparison with the phase contrast image taken at 65.7 °C (circle in Figure 7C) exhibits a significant change in the structure of the continuous crystalline PE phase. The lamellar fine structure within larger PE domains is now clearly

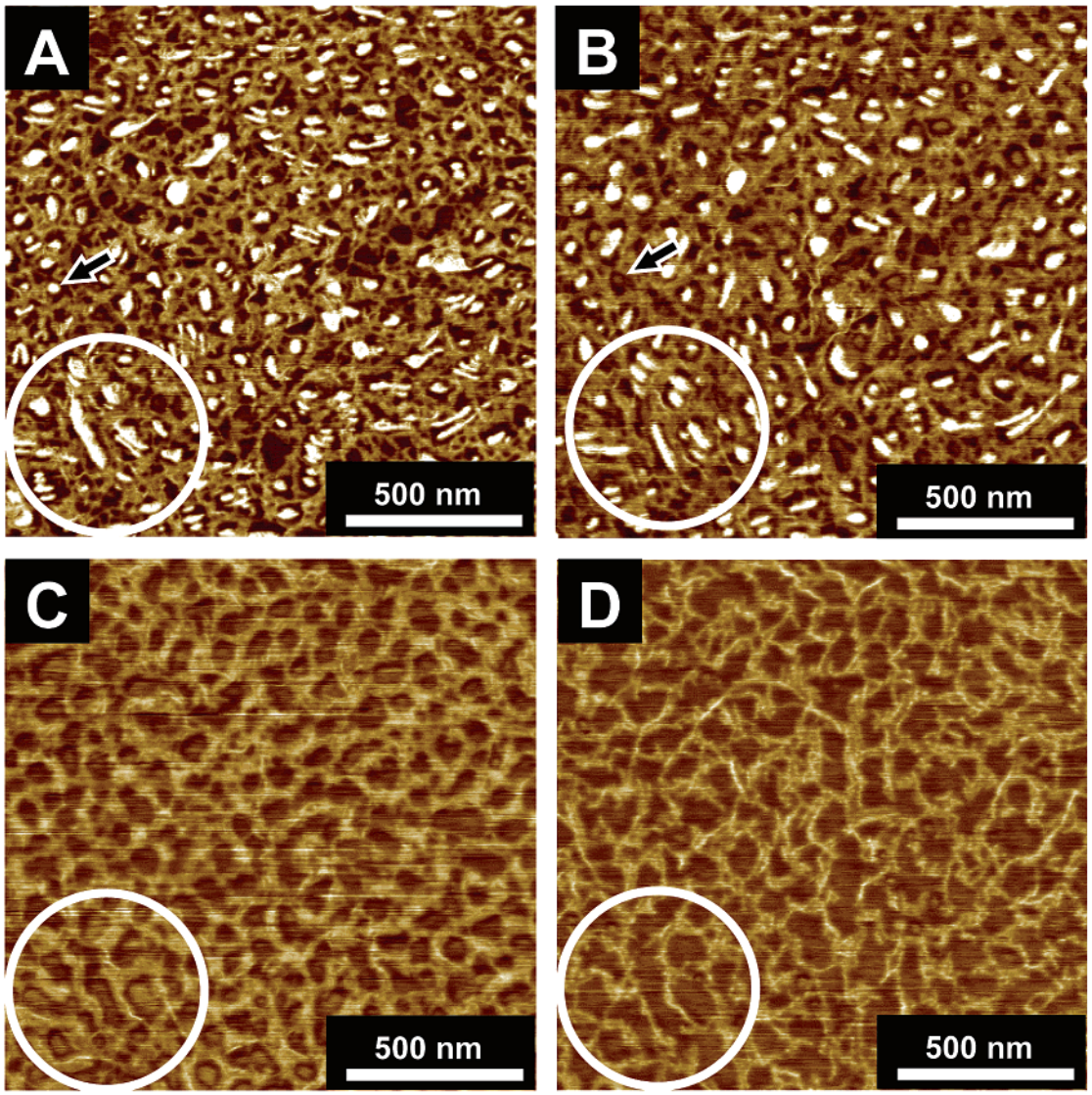

Figure 7. SFM phase contrast images of $E_{19}EP_{40}EO_{41}^{138}$ taken at 42.7 (A), 60.1 (B), 65.7 (C), and 88.7 °C (D); *z* range = 25° for all images. The phase contrast images were taken at the same spot of the thin film upon heating; identical positions are marked with a white circle for clarity. The arrows highlight a small PEO crystallite which is already molten at 60.1 °C.

visible. As a result of reorganization during annealing, the PE crystallites exhibit an almost uniform thickness (Figure 7D).

Conclusions

We have prepared several PE-*b*-PEP-*b*-PEO triblock copolymers with varying PEO content by homogeneous catalytic hydrogenation of the corresponding PB-*b*-PI-*b*-PEO triblock copolymers using Wilkinson catalyst. PB-*b*-PI-*b*-PEO triblock copolymers have been synthesized by sequential anionic polymerization in benzene, thus resulting in a high degree of 1,4-addition for the PB and PI blocks. The anionic ring-opening polymerization of ethylene oxide with Li^+ counterions was accomplished by using the strong phosphazene base *t*-BuP_4.

Thermal analysis utilizing DSC exhibits a different crystallization behavior for the PEO and PE blocks arising from different confinements active during crystallization. In PB-*b*-PI-*b*-PEO and PE-*b*-PEP-*b*-PEO triblock copolymers with PEO contents ≤ 20 wt % the PEO blocks are confined within isolated spherical or cylindrical microdomains. As a result, large supercoolings are necessary to induce crystallization of PEO. The observed crystallization temperatures (−21 to −25 °C) in combination with self-nucleation experiments point to a weak nucleation of the microdomain interphase active upon PEO crystallization. In contrast, the PE blocks in PE-*b*-PEP-*b*-PEO triblock copolymers reflect a heterogeneous nucleation mechanism, which might be attributed to the nonconfined crystallization of PE from a homogeneous mixture of PE and PEP segments in the melt.

TEM investigations on $E_{18}EP_{57}EO_{25}^{133}$ and $E_{19}EP_{40}EO_{41}^{138}$ reveal a cylindrical microstructure for the PEO blocks. The PE microstructure can be visualized by using a $E_{19}EP_{40}EO_{41}^{138}$ triblock copolymer containing residual olefinic double bonds within the PEP block, which can be selectively stained with OsO_4. In contrast to the cylindrical PEO microstructure, the PE block forms a continuous crystalline PE phase within the PEP matrix.

SFM investigations on thin films of PE-*b*-PEP-*b*-PEO triblock copolymers prepared from toluene solutions demonstrate the formation of a continuous crystalline PE phase arising from gelation upon film preparation.

The PEO blocks form molten PEO spheres or cylinders in between the crystalline PE lamellae in triblock copolymers with PEO contents <20 wt %. In $E_{19}EP_{40}EO_{41}{}^{138}$ the PEO blocks crystallize within the restricted space provided in between the continuous crystalline PE phase. Utilizing hot-stage SFM measurements, we were able to follow the melting of PEO domains and the annealing of PE crystallites upon heating of a thin film of $E_{19}EP_{40}EO_{41}{}^{138}$.

Acknowledgment. The authors thank A. Böker and Prof. G. Krausch (Physikalische Chemie II) for support concerning the SFM measurements, R. Lange (BASF AG) and Charles C. Han (NIST) for helpful discussions, and A. Göpfert (Makromolekulare Chemie II) for TEM investigations. Financial support by the German Israeli Foundation for Scientific Research and Development, DSM Research (Geleen), the Sonderforschungsbereich 481 funded by the Deutsche Forschungsgemeinschaft (DFG), and the Bayreuther Institut für Makromolekülforschung (BIMF) is gratefully acknowledged.

References and Notes

(1) Loo, Y.-L.; Register, R. A.; Ryan, A. J. *Macromolecules* **2002**, *35*, 2365.
(2) Rangarajan, P.; Register, R. A.; Adamson, D. H.; Fetters, L. J.; Bras, W.; Naylor, S.; Ryan, A. J. *Macromolecules* **1995**, *28*, 1422.
(3) Hamley, I. W.; Patrick, J.; Fairclough, A.; Terrill, N. J.; Ryan, A. J.; Lipic, P. M.; Bates, F. S.; Towns-Andrews, E. *Macromolecules* **1996**, *29*, 8835.
(4) Müller, A. J.; Balsamo, V.; Arnal, M. L.; Jakob, T.; Schmalz, H.; Abetz, V. *Macromolecules* **2002**, *35*, 3048.
(5) Quiram, D. J.; Register, R. A.; Marchand, G. R.; Ryan, A. J. *Macromolecules* **1997**, *30*, 8338.
(6) Rohadi, A.; Endo, R.; Tanimoto, S.; Sasaki, S.; Nojima, S. *Polym. Int.* **2000**, *32*, 602.
(7) Arnal, M. L.; Balsamo, V.; López-Carrasquero, F.; Contreras, J.; Carrillo, M.; Schmalz, H.; Abetz, V.; Laredo, E.; Müller, A. J. *Macromolecules* **2001**, *34*, 7973.
(8) Zhu, L.; Mimnaugh, B. R.; Ge, Q.; Quirk, R. P.; Cheng, S. Z. D.; Thomas, E. L.; Lotz, B.; Hsiao, B. S.; Yeh, F.; Liu, L. *Polymer* **2001**, *42*, 9121.
(9) Loo, Y.-L.; Register, R. A.; Ryan, A. J.; Dee, G. T. *Macromolecules* **2001**, *34*, 8968.
(10) Chen, H.-L.; Hsiao, S.-C.; Lin, T.-L.; Yamauchi, K.; Hasegawa, H.; Hashimoto, T. *Macromolecules* **2001**, *34*, 671.
(11) Nojima, S.; Toei, M.; Hara, S.; Tanimoto, S.; Sasaki, S. *Polymer* **2002**, *43*, 4087.
(12) Liu, L.-Z.; Yeh, F.; Chu, B. *Macromolecules* **1996**, *29*, 5336.
(13) Shiomi, T.; Tsukada, H.; Takeshita, H.; Takenaka, K.; Tezuka, Y. *Polymer* **2001**, *42*, 4997.
(14) Loo, Y.-L.; Register, R. A.; Adamson, D. H. *J. Polym. Sci., Part B: Polym. Phys.* **2000**, *38*, 2564.
(15) Weimann, P. A.; Hajduk, D. A.; Chu, C.; Chaffin, K. A.; Brodil, J. C.; Bates, F. S. *J. Polym. Sci., Part B: Polym. Phys.* **1999**, *37*, 2053.
(16) Kim, G.; Han, C. C.; Libera, M.; Jackson, C. L. *Macromolecules* **2001**, *34*, 7336.
(17) Buzdugan, E.; Ghioca, P.; Stribeck, N.; Beckman, E. J.; Serban, S. *Macromol. Mater. Eng.* **2001**, *286*, 497.
(18) Balsamo, V.; Paolini, Y.; Ronca, G.; Müller, A. J. *Macromol. Chem. Phys.* **2000**, *201*, 2711.
(19) Bailey, T. S.; Pham, H. D.; Bates, F. S. *Macromolecules* **2001**, *34*, 6994.
(20) Floudas, G.; Reiter, G.; Lambert, O.; Dumas, P. *Macromolecules* **1998**, *31*, 7279.
(21) Schmalz, H.; Abetz, V.; Lange, R.; Soliman, M. *Macromolecules* **2001**, *34*, 795.
(22) Schmalz, H.; Böker, A.; Lange, R.; Krausch, G.; Abetz, V. *Macromolecules* **2001**, *34*, 8720.
(23) Esswein, B.; Molenberg, A.; Möller, M. *Macromol. Symp.* **1996**, *107*, 331.
(24) Esswein, B.; Möller, M. *Angew. Chem.* **1996**, *108*, 703.
(25) Esswein, B.; Steidl, N. M.; Möller, M. *Macromol. Rapid Commun.* **1996**, *17*, 143.
(26) Förster, S.; Krämer, E. *Macromolecules* **1999**, *32*, 2783.
(27) Floudas, G.; Vazaiou, B.; Schipper, F.; Ulrich, R.; Wiesner, U.; Iatrou, H.; Hadjichristidis, N. *Macromolecules* **2001**, *34*, 2947.
(28) Zhu, L.; Cheng, S. Z. D.; Calhoun, B. H.; Ge, Q.; Quirk, R. P.; Thomas, E. L.; Hsiao, B. S.; Yeh, F.; Lotz, B. *Polymer* **2001**, *42*, 5829.
(29) Hahn, S. F. *J. Polym. Sci., Part A: Polym. Chem.* **1992**, *30*, 397.
(30) Brandrup, J.; Immergut, E. H. *Polymer Handbook*, 3rd ed.; Wiley: New York, 1989.
(31) Lanzendörfer, M.; Schmalz, H.; Abetz, V.; Müller, A. H. E. *Polym. Prepr. (Am. Chem. Soc., Div. Polym. Chem.)* **2001**, *42*, 329. Lanzendörfer, M. G.; Schmalz, H.; Abetz, V.; Müller, A. H. E. Application of FT-NIR Spectroscopy for Monitoring the Kinetics of Living Polymerizations. In *In-Situ Spectroscopy of Monomer and Polymer Synthesis*; Puskas, J. E., Storey, R., Eds.; Kluwer Academic/Plenum: New York/Dordrecht, in press.
(32) Schalz, H.; Lanzendörfer, M. G.; Abetz, V.; Müller, A. H. E. *Macromol. Chem. Phys.*, submitted.
(33) Wunderlich, B. *Macromolecular Physics*; Academic Press: New York, 1980; Vol. 3.
(34) Schmalz, H.; Müller, A. J.; Abetz, V. *Macromol. Chem. Phys.*, accepted.
(35) Bates, F. S.; Schultz, M. F.; Rosedale, J. H. *Macromolecules* **1992**, *25*, 5547.
(36) Rangarajan, P.; Register, R. A.; Fetters, L. J. *Macromolecules* **1993**, *26*, 4640.
(37) Kofinas, P.; Cohen, R. E. *Macromolecules* **1994**, *27*, 3002.
(38) Ryan, A. J.; Hamley, I. W.; Bras, W.; Bates, F. S. *Macromolecules* **1995**, *28*, 3860.
(39) Takahashi, Y.; Tadokoro, H. *Macromolecules* **1973**, *6*, 672.
(40) Howard, P. R.; Crist, B. *J. Polym. Sci., Part B: Polym. Phys.* **1989**, *27*, 2269.
(41) Sauer, B. B.; McLean, R. S.; Thomas, R. R. *Polym. Int.* **2000**, *49*, 449.
(42) Schultz, J. M.; Miles, M. J. *J. Polym. Sci., Part B: Polym. Phys.* **1998**, *36*, 2311.
(43) Beekmans, L. G. M.; Vancso, G. J. *Polymer* **2000**, *41*, 8975.
(44) Beekmans, L. G. M.; Vancso, G. J. *Polym. Mater. Sci. Eng.* **1999**, *81*, 260.
(45) Hobbs, J. K.; Miles, M. J. *Macromolecules* **2001**, *34*, 353.
(46) Lu, W.; Debelak, K.; Yang, C.; Collins, W. E.; Witt, A.; Lott, C. *Polym. Mater. Sci. Eng.* **1999**, 273.
(47) Beake, B. D.; Brewer, N. J.; Leggett, G. J. *Macromol. Symp.* **2001**, *167*, 101.
(48) Bliznyuk, V. N.; Kirov, K.; Assender, H. E.; Briggs, G. A. D.; Tsukahara, Y. *Polym. Prepr. (Am. Chem. Soc., Div. Polym. Chem.)* **2000**, *41*, 1489.
(49) Sasaki, S.; Sakaki, Y.; Takahara, A.; Kajiyama, T. *Polymer* **2002**, *43*, 3441.
(50) Pearce, R.; Vancso, G. J. *Macromolecules* **1997**, *30*, 5843.
(51) Pearce, R.; Vancso, G. J. *Polymer* **1998**, *39*, 1237.
(52) Li, L.; Chan, C.-M.; Yeung, K. L.; Li, J.-X.; Ng, K.-M.; Lei, Y. *Macromolecules* **2001**, *34*, 316.
(53) Reiter, G.; Castelein, G.; Sommer, J.-U. *Phys. Rev. Lett.* **2001**, *86*, 5918.
(54) Reiter, G.; Sommer, J.-U. *J. Chem. Phys.* **2000**, *112*, 4376.
(55) Taguchi, K.; Miyaji, H.; Izumi, K.; Hoshino, A.; Miyamoto, Y.; Kokawa, R. *Polymer* **2001**, *42*, 7443.
(56) Hamley, I. W.; Wallwork, M. L.; Smith, D. A.; Fairclough, J. P. A. *Polymer* **1998**, *39*, 3321.
(57) Reiter, G.; Castelein, G.; Hoerner, P.; Riess, G.; Blumen, A.; Sommer, J.-U. *Phys. Rev. Lett.* **1999**, *83*, 3844.
(58) Reiter, G.; Castelein, G.; Hoerner, P.; Riess, G.; Sommer, J.-U.; Floudas, G. *Eur. Phys. J.* **2000**, *E2*, 319.
(59) Reiter, G.; Castelein, G.; Sommer, J.-U.; Röttele, A.; Thurn-Albrecht, T. *Phys. Rev. Lett.* **2001**, *87*, 226101.
(60) Balsamo, V.; Collins, S.; Hamley, I. W. *Polymer* **2002**, *43*, 4207.

MA020983F